Protocadherins Mediate Dendritic Self-Avoidance in the Mammalian Nervous System

Published in final edited form as:
Nature. 2012 August 23; 488(7412): 517–521. doi:10.1038/nature11305.

PROTOCADHERINS MEDIATE DENDRITIC SELF-AVOIDANCE IN THE MAMMALIAN NERVOUS SYSTEM

Julie L. Lefebvre[1], **Dimitar Kostadinov**[1], **Weisheng V. Chen**[2], **Tom Maniatis**[2], and **Joshua R. Sanes**[1,*]

[1]Center for Brain Science and Department of Molecular and Cellular Biology, Harvard University, 52 Oxford Street, Cambridge, MA 02138

[2]Department of Biochemistry and Molecular Biophysics, Columbia University Medical Center, 701 W 168th Street, New York, NY 10032

Abstract

Dendritic arbors of many neurons are patterned by a process called self-avoidance, in which branches arising from a single neuron repel each other[1-7]. By minimizing gaps and overlaps within the arbor, self-avoidance facilitates complete coverage of a neuron's territory by its neurites[1-3]. Remarkably, some neurons that display self-avoidance interact freely with other neurons of the same subtype, implying that they discriminate self from non-self. Here, we demonstrate roles for the clustered protocadherins (Pcdhs) in dendritic self-avoidance and self/non-self discrimination. The *Pcdh* locus encodes ~60 related cadherin-like transmembrane proteins, at least some of which exhibit isoform-specific homophilic adhesion in heterologous cells and are expressed stochastically and combinatorially in single neurons[7-11]. Deletion of all 22 *Pcdh*s in the mouse gamma subcluster (*Pcdhg*s) disrupts self-avoidance of dendrites in retinal starburst amacrine cells (SACs) and cerebellar Purkinje cells. Further genetic analysis of SACs showed that Pcdhgs act cell-autonomously during development, and that replacement of the 22 Pcdhgs with a single isoform restores self-avoidance. Moreover, expression of the same single isoform in all SACs decreases interactions among dendrites of neighboring SACs (heteroneuronal interactions). These results suggest that homophilic Pcdhg interactions between sibling neurites (isoneuronal interactions) generate a repulsive signal that leads to self-avoidance. In this model, heteroneuronal interactions are normally permitted because dendrites seldom encounter a matched set of Pcdhgs unless they emanate from the same soma. In many respects, our results mirror those reported for *Dscam1* in *Drosophila*: this complex gene encodes thousands of recognition molecules that exhibit stochastic expression and isoform-specific interactions, and mediate both self-avoidance and self/non-self discrimination[4-7,12-15]. Thus, although insect Dscams and vertebrate Pcdhs share no sequence homology, they appear to underlie similar strategies for endowing neurons with distinct molecular identities and patterning their arbors.

The 58 genes of the mouse *Pcdh* locus are tandemly arranged in α, β and γ subclusters, called *Pcdha, Pcdhb* and *Pcdhg*, which encode 14, 22 and 22 cadherin-like proteins respectively[8] (Fig. 1a). In the *Pcdha* and *g* subclusters, single variable exons encoding extracellular, transmembrane and juxtamembrane domains are spliced to 3 constant exons,

*For correspondence: sanesj@mcb.harvard.edu.

AUTHOR CONTRIBUTION

J.L.L., D.K., and J.R.S. designed experiments and prepared the manuscript. J.L.L. and D.K. performed experiments and data analysis. J.R.S. supervised the project. W.V.C. and T.M. generated $Pcdhg^{tako}$ and $Pcdhg^{tcko}$ mice. All authors commented on the manuscript. The authors declare no competing interests. Correspondence and requests for materials should be addressed to J.R.S. (sanesj@mcb.harvard.edu).

generating proteins with unique extracellular but common intracellular domains[8]. The complexity of this locus is reminiscent of that of *Dscam1*, which mediates self-avoidance in *Drosophila*[4-7,15]. Moreover, *Pcdh*s, like *Dscam1*, exhibit isoform-specific homotypic recognition and stochastic, combinatorial expression[13,14]. In contrast, the two vertebrate *Dscam*s are not complex genes, so although they mediate both repulsive and attractive interactions among neurons[16-19], they are unlikely to underlie self/non-self discrimination. We therefore investigated roles of *Pcdh*s in these processes.

Previous studies of mouse mutants lacking all 22 *Pcdhg* genes revealed that they are required for survival of multiple neuronal types[20-23]. To seek roles of Pcdhgs in self-avoidance, we focused on a retinal interneuron, the starburst amacrine cell (SAC), which expresses *Pcdhgs*[22] and exhibits dramatic dendritic self-avoidance[24]. Radially symmetric SAC dendritic arbors are confined to narrow planes within the inner plexiform (synaptic) layer; SACs have no axons. Dendrites of a single SAC seldom cross one another, yet dendrites of neighboring SACs cross freely (Fig. 1b, c; Supplementary Fig. 1) and even form synapses with each other[24,25], suggesting that they can distinguish “self” from “non-self.”

We used a conditional mutant (*Pcdhg*^{fcon3})[22] to bypass the neonatal lethality of constitutive *Pcdhg* mutants and employed Cre drivers that delete *Pcdhg*s from all or subsets of retinal cells. We visualized individual neurons by infection with recombinant adeno-associated virus (rAAV) expressing a fluorescent protein (XFP; Fig. 1d), biolistic delivery of DNA encoding XFP, or intracellular injection of a fluorescent dye. We identified SACs, the sole cholinergic neurons in retina, with antibodies to choline acetytransferase (ChAT), which also demonstrated the association of XFP-positive SAC dendrites with dendrites from other (XFP-negative) SACs (Supplementary Figs. 1 and 2).

SAC morphology was profoundly altered in *Pcdhg* mutant retinas (*Pcdhg*$^{fcon3/fcon3}$*; retina-cre*, called *Pcdhg*$^{rko/rko}$ here; see online Methods for genotypes). Dendrites arising from a single SAC frequently crossed each other and sometimes formed loose bundles (Fig. 1f-i and Supplementary Fig. 1). Crossing frequency was increased several-fold in both proximal and distal regions of the arbor (Fig. 1j). These defects were highly specific in that the diameter of SAC arbors, the number of dendritic termini, the laminar targeting of SAC dendrites, heteroneuronal interactions among dendrites, and the mosaic arrangement of SAC bodies were all unaffected in *Pcdhg*$^{rko/rko}$ mutants (Fig. 1k, l and Supplementary Figs. 1 and 2). Thus, Pcdhgs are dispensable for many aspects of SAC morphogenesis but required for their self-avoidance.

In the absence of *Pcdhgs*, neurons of many types die in elevated numbers during the period of naturally-occurring cell death[21,22]. Although SACs are largely spared in *Pcdhg* mutants[22], their dendritic defects might be secondary to loss of other neurites with which they ordinarily interact. To test this possibility, we blocked apoptosis by deleting the *Bax* gene, which is required for naturally occurring and *Pcdhg*-dependent neuronal death[22,23,26]. SAC morphology was normal in *Bax*$^{-/-}$ mice, but self-avoidance defects persisted in *Bax*$^{-/-}$; *Pcdhg*$^{rko/rko}$ double mutants (Supplementary Fig.3).

We next asked whether Pcdhgs are required for the development of SAC arbors, or only for their maintenance. In wild-type neonates, SACs extended dendrites that branched profusely and contacted each other (Fig. 2a-c). By P12, however, excess neurites and isoneuronal contacts were eliminated, resulting in a radial arbor with evenly-spaced branches (Fig. 2d and see ref. 24). Thus, self-avoidance arises rapidly following a short period of isoneuronal “sampling.” In *Pcdhg*$^{rko/rko}$ mice, SACs were clearly aberrant by P3, exhibiting excessive crossing and tangling of neurites (Fig. 2e-g). Excess branches were subsequently eliminated, but whereas most crossing branches were eliminated in controls, many persisted in mutants

(Fig. 2h). Thus, Pcdhgs may lead to self-avoidance by mediating repulsive interactions that bias the rearrangement process to selectively eliminate contacts among isoneuronal branches.

To initiate analysis of the mechanism by which Pcdhgs mediate self-avoidance, we next asked whether they act cell-autonomously. We selectively removed *Pcdhg*s from SACs using a ChAT-Cre line. In this case, *Pcdhg*-negative SACs were surrounded by *Pcdhg*-positive neurons of other types. We also deleted *Pcdhg*s from individual SACs using a transgenic line that expressed tamoxifen-activated Cre recombinase in SACs; we activated Cre with a low dose of tamoxifen and introduced a Cre-dependent reporter to mark mutant SACs. In this case, *Pcdhg*-negative SACs were surrounded by *Pcdhg*-positive SACs. In both cases, SACs lacking *Pcdhg*s exhibited striking self-avoidance defects (Supplementary Fig. 4). To test whether Pcdhgs can act in completely isolated SACs, we used fluorescence-activated cell sorting to purify SACs from a transgenic line in which they are selectively labeled by an orange fluorescent protein (Thy1-OFP3) and cultured them at low density. Isolated SACs extended dendrites that formed radial, web-like arbors (Fig. 2i) reminiscent of those observed at ~P5 in vivo (Fig. 2b). In contrast, SACs from $Pcdhg^{rko/rko}$; *Thy1-OFP3* mice exhibited less symmetrical and unevenly spaced arbors, reminiscent of those observed in $Pcdhg^{rko/rko}$ retinas at P5 (Fig. 2j and Supplementary Fig. 5). Analysis of space-filling capacity of dendritic arbors[2,27] (see Methods) revealed that defects in vitro were similar in magnitude to those in vivo (Fig. 2k,l). Thus, Pcdhgs do not depend on intercellular interactions to promote self-avoidance.

We next assessed the requirement for isoform diversity in Pcdhg-dependent self-avoidance. We used RT-PCR to survey expression of *Pcdhg* isoforms in whole retina, in amacrines generally, and in SACs specifically. All 22 *Pcdhg* variants were expressed in each preparation, with no indication of decreased diversity in purified subpopulations (Supplementary Fig. 6). We then analyzed a targeted mouse mutant, $Pcdhg^{tcko}$, in which three contiguous *Pcdhg* variable exons, C3-C5, had been deleted. Expression of the remaining 19 *Pcdhg* isoforms is unperturbed in this allele [28]. Because $Pcdhg^{tcko}$ homozygous mice die at birth [28]}, we generated transheterozygous animals ($Pcdhg^{tcko/fcon3}$;*retina-cre*) so that only retina lack both copies of *Pcdhgc3-c5*. In these retinas, neuronal death was as prevalent as in those of $Pcdhg^{rko/rko}$ mice[29], yet SACs exhibited normal self-avoidance (Fig. 3a,e).

In a complementary approach, we generated a line in which the single PcdhgC3 isoform, fused to a fluorescent protein (mCherry), could be expressed in any cell in a Cre-dependent manner (*ROSA26-CAG::lox-Stop-lox-Pcdhgc3-mCherry* or *cC3-mCherry*). Thus, in *cC3-mCherry*;$Pcdhg^{rko/rko}$ mice, *Cre* both deletes all 22 endogenous *Pcdhg* genes and activates the single PcdhgC3-mCherry isoform throughout the retina. Analysis of mCherry fluorescence confirmed Cre-dependent expression of the transgene in all retinal cells and appropriate localization of the fusion protein to cell membranes and synaptic layers (Supplementary Fig. 7). Expression of *Pcdhgc3* alone rescued self-avoidance defects of *Pcdhg* mutants (Fig. 3b,e).

To test the possibility that only some isoforms are dispensable for self-avoidance, we analyzed a second set of isoforms. We generated $Pcdhg^{tako}$, which lacks the *Pcdhga1-a3* variable exons[28], and a line that expresses *Pcdhga1-mCherry* in a Cre-dependent manner (*cA1-mCherry*). Results were similar to those for the C3-5 group: self-avoidance persisted in the absence of PcdhgA1-A3 and was rescued by replacement of all Pcdhg isoforms with PcdhgA1 alone (Figs. 3c-e and Supplementary Fig. 7). From these results, we conclude that no single Pcdhg isoform is necessary but any single isoform is sufficient for dendritic self-avoidance.

Although Pcdhg isoform diversity is not required for isoneuronal self-avoidance, it may be required to ensure that dendrites of adjacent SACs do not avoid each other, which would prevent them from interacting. The ability to generate a SAC population expressing a single Pcdhg isoform (*Pcdhga1* or *Pcdhgc3*) enabled us to test this idea. We injected closely spaced pairs of SACs with different fluorophores (Fig. 4a) and measured the extent to which their dendrites overlapped. To determine whether this method reliably revealed interactions among SACs, we rotated, flipped or rotated and flipped the image of one of the cells, and recalculated overlap. Only the real image showed an overlap greater than that of the manipulated images (Fig. 4b). We then measured overlap for pairs of SACs from wild-type, mutant and single isoform-expressing mice, normalizing for intercellular distance by comparing overlap to the value calculated from the flipped image (Fig. 4c-e and Supplementary Fig. 8). Overlap was equivalent in wild-type and mutant retina, but significantly decreased in retinas expressing a single isoform (Fig. 4f); values for *Pcdhga1* and *Pcdhgc3* were similar (1.01 and 1.08). Likewise, the mean length of overlapping segments was greater than expected for random overlap in wild-type and mutant but not in single isoform-expressing pairs (Fig. 4g). Thus, when all SACs express the same *Pcdhg* isoform, heteroneuronal dendrites avoid each other, just as isoneuronal dendrites do in control SACs. We conclude that isoform diversity enables SACs to distinguish isoneuronal from heteroneuronal dendrites.

Finally, we asked whether Pcdhgs mediate self-avoidance in areas other than retina. We examined cerebellar Purkinje cells, which have elaborate, planar dendritic arbors known to exhibit self-avoidance[3] (Fig. 5a-c). Importantly, stochastic and combinatorial expression, which underlies the ability of *Drosophila Dscam1* to mediate self-avoidance[4-6,12,14,15,29], has been documented for Pcdhgs in Purkinje cells[10]. We selectively deleted *Pcdhgs* from Purkinje neurons using an *L7-cre* transgene, marked cells with a vector that expresses fluorescent proteins in a Cre-dependent manner, and examined them at P15, P21 and at P35, after arbors have matured[30]. Deletion of *Pcdhg*s from Purkinje cells had no detectable effect on their survival, shape, size or branching pattern (Fig. 5d,e,h,i and Supplementary Fig. 9), but their arbors were disorganized and dendrites often crossed over each other (Fig. 5f, g). Use of a Cre-dependent reporter revealed that deletion remained incomplete at P8, at which time Purkinje dendrite growth was already advanced (Supplementary Fig. 9). It is therefore possible that earlier deletion of *Pcdhg*s would lead to a more dramatic effect. Nonetheless, these results demonstrate a role for *Pcdhg*s in Purkinje cell self-avoidance.

In summary, although vertebrate *Pcdhs* and *Drosophila Dscam1* are structurally unrelated, they have remarkable parallels: both encode numerous isoforms from a single locus, the isoforms are expressed stochastically and combinatorially, and the encoded proteins interact homophilically[7,8,10-14]. We have now shown that in mammalian neurons, Pcdhgs, like Dscam1[4-6,12], promote self-avoidance during development by a cell-autonomous mechanism. In addition, for both *Dscam1* and *Pcdhgs*, diversity appears to underlie self/non-self discrimination, presumably because neighboring neurons are unlikely to express the same isoforms and are therefore free to interact[7,12,14,15]. Thus, two phyla appear to have recruited different molecules to mediate similar, complex strategies for self-recognition during formation of neuronal arbors. These parallels also raise the question of why vertebrate and invertebrate nervous systems have invested heavily in mechanisms that promote self-avoidance. In principle, self-avoidance allows neurons to cover their receptive or projective fields maximally while retaining the ability to overlap those of neighboring neurons[1-3]. However, to our knowledge, the effect of perturbing self-avoidance on circuit function has yet to be assessed in any system. We can now address this issue by electrophysiological analysis of SACs, Purkinje cells, and their synaptic targets in *Pcdhg* mutant mice.

METHODS SUMMARY

Transgenic, knock-out and knock-in mouse lines used for this study, as well as methods for marking cells are described in online Methods. Identity of labeled SACs was confirmed by immunolabeling retinas for the cholinergic neuron-specific marker. Dendrite self-crossings were quantified by number of branch overlaps detected in single confocal planes.

METHODS

Mouse strains

The *Pcdhg* ^{fcon3} conditional mutant allele, in which the third constant exon is flanked by loxP sequences and which generates a functionally null allele following Cre recombination, was described previously[21,22]. Retina-specific *Chx10-cre*[31] and *Six3-cre* transgenic mice[32] were provided by Constance Cepko (Harvard) and William Klein (M.D. Anderson Cancer Center) respectively. *Bax*$^{-/-}$ mutants[33], Purkinje-specific *L7Bac-cre* transgenic mice[34], *Chat-cre*, in which the Cre recombinase gene was targeted to the endogenous ChAT gene[35], and Rosa-CAG-LoxP-STOP-LoxP-tdTomato-WPRE reporter mice[36] were obtained from Jackson Laboratories. A line of BAC transgenic mice in which regulatory elements from the *fstl4* gene drive expression of CreER was generated as described in ref. 37. In this line, called line 1 to distinguish it from the line called "BD" in ref. 37, CreER was expressed in SACs, as well as sparse other amacrine cells. We believe that expression reflects influences at the site of transgene integration rather than expression of *fstl4*. Thy1-OFP3 transgenic mice, in which Thy1 promoter and regulatory elements direct expression of Kusabira Orange (OFP) in SACs and subset of RGCs, were described previously[37]. Pcdhg^{tcko} and Pcdhg^{tako} mice were generated using standard gene targeting techniques[28]. Mice were maintained on a C57/B6J background. All experiments were carried out in accordance with protocols approved by the Harvard University Standing Committee on the Use of Animals in Research and Teaching.

Generation of single Pcdhg isoform conditional knock-in mice

Pcdhga1 and *pcdhgc3* full-length cDNAs were amplified from RNA isolated from P21 C57/BL6 mouse brain, and cloned in frame into pCMV-mCherry-N1 (Clontech). Linker sequence residing between the 3rd constant exon and *gfp* in Pcdhg^{fusg} knock-in mice and shown to produce functional Pcdhg-GFP fusion proteins *in vivo*[20] was subcloned into pCMV-pcdhga1/c3-mCherry-N1. Targeting vector pRosa26-PAS[38] was modified as described in ref. 40 to include a CAG cassette (chicken β-actin promoter and CMV immediate-early enhancer), a Gateway RfA destination site (Invitrogen), a WPRE fragment (woodchuck hepatitis virus posttranscriptional element), and a STOP sequence was cloned from pBS302[39] (Addgene plasmid 11925). LoxP-STOP-loxP-Pcdhga1/c3-mCherry was recombined into pROSA26-CAG-Rfa-WPRE-FNF-iSceI, creating pROSA26-CAG-loxP-STOP-loxP-Pcdhga1/c3-mCherry-WPRE-FNF-iSceI targeting vectors. The iSceI- linearized vectors were electroporated into 129/B6 F1 hybrid ES cell line V6.5. G418-resistant, targeted ES clones were identified by PCR: 1.7 kb fragment amplified by 5′armRosa-F: GGCGGACTGGCGGGACTA and 5′armCAG-R: CCAGGCGGGCCATTTACCGTAAG; and 9.1kb fragment amplified by 3′armCherryF: CTCCCACAACGAGGACTACACCATC and 3′armRosaR: GCATTTTAAAAGCATGAAACTACAAC. ES cell transfections and blastocyst injections were performed by the Genome Modification Facility, Harvard University. Following germ-line transmission, the FRT-neo-FRT cassette was excised by crossing to mice that express Flp recombinase ubiquitously[40]. Gt(ROSA)26Sor::CAG-loxP-STOP-loxP-Pcdhga1/c3-mCherry conditional knock-in mice are called *cA1-mCherry* and *cC3-mCherry.*

Labeling of neurons

Plasmid encoding pAAV2/2-CAG-palmitoylation tag-mCherry-WPRE was used to generate recombinant AAV2/2 expressing membrane-tagged Cherry. To label SACs in retina expressing *cC3-mCherry* or *cA1-mCherry*, we used rAAV2/2-CBA-YC3.6-WPRE expressing a calcium sensor that includes cytosolic YFP and used here for visualization of neuronal morphology[41]. Recombinant AAV2/2-CAG-memb-mCherry and rAAV2/2-YC3.6 were prepared at the Harvard Gene Therapy Institute ($1–2 \times 10^{12}$ genome copies/mL, Boston, MA). Optimal titers of $1–2 \times 10^{9}$ viral genome particles/mL for AAV2/2-CAG-memb-mCherry and 2×10^{10} viral genome particles/mL for rAAV2/2- YC3.6 were prepared in phosphate-buffered saline (PBS, pH = 7.4). rAAV2/9 expressing GFP and mCherry were generated and generously provided by Dawen Cai and Kimberly Cohen in our laboratory; high titer virus was produced at the University of Pennsylvania Vector Core.

To inject virus into eyes, adult mice were anesthetized with ketamine/xylazine by intraperitoneal injection. A 30½G needle was used to make a small hole in the temporal eye, below the cornea, and 1.5 μL of rAAV virus was injected into the vitreous humor with a Hamilton syringe and 33G blunt-ended needle. Animals were euthanized and retinas were dissected 4-6 weeks following injection. For cerebellar virus infection, P1-P2 mice were anesthetized with ice and a small puncture was made into caudal-medial position of one cortical lobe; 1.5 μL of rAAV2/9-GFP; mCherry virus was injected with a Hamilton syringe and 33G blunt-ended needle. Mice were analyzed 12 to 35 days post-infection.

For biolistic transfection of SACs, gold particles (1.0 μm diameter, Bio-Rad), were coated with plasmids encoding tdTomato driven by CMV promoter[24]. Live retinas were dissected, transected with four radial incisions, flattened with photoreceptor side down, and mounted onto a nitrocellulose filter (Millipore). Gold particles were delivered using a Biolistics Helios Gene gun device (Bio-Rad), and retinas were cultured in Ames medium (Sigma) in an oxygenated incubator heated to 37°C for 12-16 hrs.

To assess interactions between dendrites of neighboring SACs, we injected pairs of cells with fluorescent dyes. Retinas from mice expressing OFP in SACs (Thy1-OFP3) were mounted RGC side up and perfused with Ames medium bubbled with $95\%O_2/5\%CO_2$ at 25°C. OFP^+ SACs were visualized with epifluorescence, and impaled with high resistance electrodes (50 MΩ) filled with a K^+ based intracellular recording solution supplemented with 50 μM Alexa Fluor 568 (for targeting) and 200 μM of Alexa Fluor 488 or 647 (for filling, Invitrogen). Square voltage pulses of ~3V were applied to SACs at 50 Hz using a BK Precision Model 3011B function generator. After filling one SAC, the electrode was replaced with a second containing the contrasting dye and the second cell was filled. Images of labeled SAC pairs in live retinas were acquired at 40X on a Zeiss LSM 510 confocal microscope.

Tissue preparation and immunohistochemistry

Mice were euthanized with intraperitoneal injection of Nembutal, and either enucleated immediately or transcardially perfused with Ringer's solution followed by 4% paraformaldehyde (PFA) in PBS. Eye cups were removed and fixed in 4% PFA on ice for 1 hour, followed by dissection and post-fixation of retinas for an additional 30 minutes, then rinsed with PBS. Brains were post-fixed in 4% PFA at 4°C overnight. Animal procedures were in compliance with the US National Institutes of Health Guide for the Care and Use of Laboratory Animals and approved by the Animal and Care and Use Program at Harvard University.

Wholemount preparations and cryosections of retinas were performed as described[22,42]. Briefly, whole retinas were incubated for 1-2 hours in blocking buffer (0.4% Triton-X, 4%

normal donkey serum in PBS), then incubated for 6 days at 4°C with primary antibodies. Sagittal 80μm sections of cerebellum were obtained with a vibratome (Leica), incubated in blocking buffer, and with primary antibodies for 2 days at 4°C. Following washing, retinas and brain sections were incubated for 3 hours at room temperature with Alexa-conjugated secondary antibodies (Invitrogen or Jackson ImmunoResearch). Whole retinas were flattened with photoreceptor side down onto nitrocellulose filters. Retina flatmounts and brain sections were mounted onto glass slides, coverslipped with Vectashield (Vector) or Fluoromount G (Southern Biotech), and imaged on an Olympus FV1000 scanning confocal microscope. Antibodies used were as follows: chick and rabbit anti-GFP (Aves and Millipore); rabbit anti-DsRed (Clontech); goat anti-choline acetyltransferase (Millipore); guinea pig anti-vGluT3 (Millipore); rabbit anti-Calbindin (Swant); mouse anti-syntaxin HPC1 clone (Sigma); rabbit anti-cleaved caspase3 (Cell Signaling Technology). Nuclei were labeled with DAPI, Po-pro1, or NeuroTrace Nissl 435/455 (Invitrogen).

SAC purification and culture

To isolate and culture wild-type and *Pcdhg* mutant SACs *in vitro,* we crossed the Thy1-OFP3 transgene, which selectively directs expression of Kusabira Orange (OFP) in SACs and subset of RGCs[37], into *Pcdhg*^{fcon3}*; Six-cre* mice. Retinas from genotyped *Pcdhg*$^{fcon3/fcon3}$*; Six-cre* Thy1-OFP3 mutant and control P2 mice were dissociated using papain[22]. OFP^{+} SACs were isolated by fluorescence activated cell sorting (FACS, MoFlo), plated onto poly-L-lysine-coated glass coverslips (Warner) and cultured 7-9 days in RGC growth media modified from Meyer-Franke *et al.*[43] in the following ways: (a) substitution of NS21[44] for B27, (b) substitution of N2 (Invitrogen) for Sato stock, (c) addition of TGF-β1 and -β2 (2.5ng/mL; Peprotech), and (d) addition of mouse glia-conditioned medium (15%). One-third of media was exchanged with fresh media every three days. Cells were fixed with cold 4%PFA/4% Sucrose for 15min, and immunostained for syntaxin and calbindin to confirm SAC identity, and for GFP to confirm *Pcdhg*$^{-/-}$; GFP^{-} SACs from unrecombined Pcdhg-GFP^{+} SACs due to variegated Six3-Cre activity in retina.

Image Analysis

For best reproduction and clarity of SAC arbors, maximized projections of confocal images were inverted and contrast-enhanced using Photoshop (Adobe Systems Inc.). For morphometric analysis of SACs, we used Fiji software and selected confocal image series of wild-type and *Pcdhg* mutant SACs situated in comparable retinal eccentricities. Self-crossings per dendritic branch order were quantified as number of branch overlaps detected in single confocal planes; crossings occurring distal to 5′ branch order could not be quantified accurately due to severity of defects in mutants. Dendritic field diameter was measured as the longest axis of arbor. In some cases, arbors were reimaged by oversampling using a 60X 1.45NA objective at x,y,z resolution of 47 × 47 × 131and then subjected to deconvolution using Huygens software (http://www.svi.nl/HuygensProfessional).

For analysis of SAC density and mosaic regularity, confocal z-stacks of ChAT-labeled SACs through the GCL and INL were acquired at similar locations in central retina. Sample sizes were 4-5 areas (0.099mm^2) per animal, 2-4 animals per genotype. For each field, X-Y coordinates of SAC arrays were obtained by manually marking centers of cells using Fiji and used to compute SAC density (#/mm^2), packing factor[45], and Density recovery profiles (DRP)[46] with WinDRP software (http://www.mpimf-heidelberg.mpg.de/~teuler/WinDRP/ReadMe.htm).

To compare the space-filling and complexity of control and mutant SAC arbors, we computed fractal dimensions, *Df*, which provide a measure of how completely dendrites fill its area[2,27,47,48]. To calculate *Df*, we applied the box-counting method as implemented in the

FracLac 2.5 plug-in for ImageJ software (http://rsb.info.nih.gov/ij/plugins/fraclac/FLHelp/Introduction.htm.; NIH). Confocal images of cultured mutant and control SACs were obtained at equivalent laser scanning parameters with a 60X oil immersion lens, and maximum projections and thresholded, binary images were processed using Image J. Box counts using a series of progressively smaller box sizes (*d)* were scanned in a region of interest covering the SAC arbor, and the number of boxes intersected by pixels [*k(d)*] were analyzed; this computes *Df,* which represents an inverse linear regression between log[*k(d)*] and log(*d*). *Df* ranges from 1.0 (straight line with a dimension of 1) to 2.0 (plane with a dimension of 2); a difference of 0.1 represents a doubling of complexity[27].

For analysis of dendrite overlap between arbors of neighboring SACs, pairs with somata separated by 80-160 μm were selected because their dendrites are known to interact[25]. Images were processed using Fiji or Photoshop software. To estimate the amount of dendritic overlap that would occur by chance if two SAC arbors occupy the same territory, we flipped or rotated the image of one SAC, realigned cell body position, and merged images. This method was inspired by the work of Wassle and Boycott on tiling of RGC dendrites[49]. We measured total overlapping pixels in real and flipped images, interpreting ratios of >1 (real/flipped) as indicated non-random interactions between SACs.

Purkinje cell dendrite self-crossings detected in single confocal planes were counted in a 7,225 μm^2 region of interest assigned to middle of arbor. Purkinje arbor areas were measured using the convex-hull selection in Fiji. Calbindin-labeled Purkinje somata residing along a 635 μm segment in lobules III-VI in single confocal planes were counted to measure PC density.

Means were compared using two-tailed Student's *t* test on condition of equivalent variances determined by *F*-test, or with Mann-Whitney non-parametric test. Means of multiple samples were compared using ANOVA and posthoc Tukey test.

RT-PCR of dissociated retina cells

We used FACS to sort live cells from dissociated P7 whole retina, $VC1.1^+$ amacrine cells, and OFP^+;$Thy1.2^-$ SACs cells, as described previously[37,50]. Amacrine cells were sorted by selection for monoclonal VC1.1 antibody (200 μg ml^{-1}, Sigma) and an anti-IgM secondary conjugated to phycoerythrin-Cy7 (Southern) were applied to live suspension of dissociated retina cells. OFP^+ SACs were sorted from OFP^+ RGCs by negative selection of Thy1.2-PE-Cy7 labeled RGCs. In each condition, 2000 cells were sorted directly into RNA lysis buffer (Qiagen); RNA was purified and first strand cDNAs were generated with Superscript RT III (Invitrogen). Primers that uniquely detect the 22 Pcdhg variable exon-constant exon spliced transcripts were adapted from ref. 21, with modifications to avoid cross-hybridization. These primers, and others used to assess purity of the sorted population, are listed in Supplementary Table 1. PCR program used is: 94°C for 2 minutes; 30 cycles of 94°C for 20 seconds, 56°C for 30 seconds, 72°C for 1 minute; 72°C for 7 minutes.

Supplementary Material

Refer to Web version on PubMed Central for supplementary material.

Acknowledgments

We thank members of our laboratory for providing advice and reagents, including D. Cai and K. Cohen (AAV), I.-J. Kim (*fstl4*-line 1 mice) and M. Yamagata for modified ROSA-CAG targeting vector. We also thank Beth Stevens (Children's Hospital) for advice on culture methods.

This work was supported by grants from N.I.H. to J.R.S. (R01NS029169 and R01EY022073) and T.M. (R01NS043915) and NARSAD Young Investigator Award to J.L.L.

REFERENCES

1. Kramer AP, Kuwada JY. Formation of the receptive fields of leech mechanosensory neurons during embryonic development. J Neurosci. 1983; 3:2474–2486. [PubMed: 6317810]
2. Montague PR, Friedlander MJ. Expression of an intrinsic growth strategy by mammalian retinal neurons. Proc Natl Acad Sci U S A. 1989; 86:7223–7227. [PubMed: 2780566]
3. Grueber WB, Sagasti A. Self-avoidance and tiling: Mechanisms of dendrite and axon spacing. Cold Spring Harb Perspect Biol. 2010; 2:a001750. [PubMed: 20573716]
4. Matthews BJ, et al. Dendrite self-avoidance is controlled by Dscam. Cell. 2007; 129:593–604. [PubMed: 17482551]
5. Soba P, et al. Drosophila sensory neurons require Dscam for dendritic self-avoidance and proper dendritic field organization. Neuron. 2007; 54:403–416. [PubMed: 17481394]
6. Hughes ME, et al. Homophilic Dscam interactions control complex dendrite morphogenesis. Neuron. 2007; 54:417–427. [PubMed: 17481395]
7. Zipursky SL, Sanes JR. Chemoaffinity revisited: dscams, protocadherins, and neural circuit assembly. Cell. 2010; 143:343–353. [PubMed: 21029858]
8. Wu Q, Maniatis T. A striking organization of a large family of human neural cadherin-like cell adhesion genes. Cell. 1999; 97:779–790. [PubMed: 10380929]
9. Kohmura N, et al. Diversity revealed by a novel family of cadherins expressed in neurons at a synaptic complex. Neuron. 1998; 20:1137–1151. [PubMed: 9655502]
10. Kaneko R, et al. Allelic gene regulation of Pcdh-alpha and Pcdh-gamma clusters involving both monoallelic and biallelic expression in single Purkinje cells. J Biol Chem. 2006; 281:30551–30560. [PubMed: 16893882]
11. Schreiner D, Weiner JA. Combinatorial homophilic interaction between gamma-protocadherin multimers greatly expands the molecular diversity of cell adhesion. Proc Natl Acad Sci U S A. 2010; 107:14893–14898. [PubMed: 20679223]
12. Zhan XL, et al. Analysis of Dscam diversity in regulating axon guidance in Drosophila mushroom bodies. Neuron. 2004; 43:673–686. [PubMed: 15339649]
13. Wojtowicz WM, Flanagan JJ, Millard SS, Zipursky SL, Clemens JC. Alternative splicing of Drosophila Dscam generates axon guidance receptors that exhibit isoform-specific homophilic binding. Cell. 2004; 118:619–633. [PubMed: 15339666]
14. Neves G, Zucker J, Daly M, Chess A. Stochastic yet biased expression of multiple Dscam splice variants by individual cells. Nat Genet. 2004; 36:240–246. [PubMed: 14758360]
15. Hattori D, et al. Robust discrimination between self and non-self neurites requires thousands of Dscam1 isoforms. Nature. 2009; 461
16. Yamagata M, Sanes JR. Dscam and Sidekick proteins direct lamina-specific synaptic connections in vertebrate retina. Nature. 2008; 451:465–469. [PubMed: 18216854]
17. Fuerst PG, Koizumi A, Masland RH, Burgess RW. Neurite arborization and mosaic spacing in the mouse retina require DSCAM. Nature. 2008; 451:470–474. [PubMed: 18216855]
18. Fuerst PG, et al. DSCAM and DSCAML1 function in self-avoidance in multiple cell types in the developing mouse retina. Neuron. 2009; 64:484–497. [PubMed: 19945391]
19. Sanes JR, Zipursky SL. Design principles of insect and vertebrate visual systems. Neuron. 2010; 66
20. Wang X, et al. Gamma protocadherins are required for survival of spinal interneurons. Neuron. 2002; 36:843–854. [PubMed: 12467588]
21. Prasad T, Wang X, Gray PA, Weiner JA. A differential developmental pattern of spinal interneuron apoptosis during synaptogenesis: insights from genetic analyses of the protocadherin-gamma gene cluster. Development. 2008; 135:4153–4164. [PubMed: 19029045]
22. Lefebvre JL, Zhang Y, Meister M, Wang X, Sanes JR. gamma-Protocadherins regulate neuronal survival but are dispensable for circuit formation in retina. Development. 2008; 135:4141–4151. [PubMed: 19029044]

23. Weiner JA, Wang X, Tapia JC, Sanes JR. Gamma protocadherins are required for synaptic development in the spinal cord. Proc Natl Acad Sci U S A. 2005; 102:8–14. [PubMed: 15574493]
24. Stacy RC, Wong RO. Developmental relationship between cholinergic amacrine cell processes and ganglion cell dendrites of the mouse retina. J Comp Neurol. 2003; 456:154–166. [PubMed: 12509872]
25. Lee S, Zhou ZJ. The synaptic mechanism of direction selectivity in distal processes of starburst amacrine cells. Neuron. 2006; 51:787–799. [PubMed: 16982423]
26. White FA, Keller-Peck CR, Knudson CM, Korsmeyer SJ, Snider WD. Widespread elimination of naturally occurring neuronal death in Bax-deficient mice. J Neurosci. 1998; 18:1428–1439. [PubMed: 9454852]
27. Jelinek HF, Fernandez E. Neurons and fractals: how reliable and useful are calculations of fractal dimensions? J Neurosci Methods. 1998; 81:9–18. [PubMed: 9696304]
28. Chen WV, et al. Functional significance of isoform diversification in the protocadherin gamma gene cluster. Neuron. 2012 in press.
29. Wang J, et al. Transmembrane/juxtamembrane domain-dependent Dscam distribution and function during mushroom body neuronal morphogenesis. Neuron. 2004; 43:663–672. [PubMed: 15339648]
30. Kaneko M, et al. Remodeling of monoplanar Purkinje cell dendrites during cerebellar circuit formation. PLoS One. 2011; 6:e20108. [PubMed: 21655286]
31. Rowan S, Cepko CL. Genetic analysis of the homeodomain transcription factor Chx10 in the retina using a novel multifunctional BAC transgenic mouse reporter. Dev Biol. 2004; 271:388–402. [PubMed: 15223342]
32. Furuta Y, Lagutin O, Hogan BL, Oliver GC. Retina- and ventral forebrain-specific Cre recombinase activity in transgenic mice. Genesis. 2000; 26:130–132. [PubMed: 10686607]
33. Knudson CM, Tung KS, Tourtellotte WG, Brown GA, Korsmeyer SJ. Bax-deficient mice with lymphoid hyperplasia and male germ cell death. Science. 1995; 270:96–99. [PubMed: 7569956]
34. Zhang XM, et al. Highly restricted expression of Cre recombinase in cerebellar Purkinje cells. Genesis. 2004; 40:45–51. [PubMed: 15354293]
35. Rossi J, et al. Melanocortin-4 receptors expressed by cholinergic neurons regulate energy balance and glucose homeostasis. Cell Metab. 2011; 13:195–204. [PubMed: 21284986]
36. Madisen L, et al. A robust and high-throughput Cre reporting and characterization system for the whole mouse brain. Nature Neurosci. 2010; 13:133–140. [PubMed: 20023653]
37. Kay JN, et al. Retinal ganglion cells with distinct directional preferences differ in molecular identity, structure, and central projections. J Neurosci. 2011; 31:7753–7762. [PubMed: 21613488]
38. Srinivas S, et al. Expression of green fluorescent protein in the ureteric bud of transgenic mice: a new tool for the analysis of ureteric bud morphogenesis. Dev Genet. 1999; 24:241–251. [PubMed: 10322632]
39. Sauer B. Inducible gene targeting in mice using the Cre/lox system. Methods. 1998; 14:381–392. [PubMed: 9608509]
40. Farley FW, Soriano P, Steffen LS, Dymecki SM. Widespread recombinase expression using FLPeR (flipper) mice. Genesis. 2000; 28:106–110. [PubMed: 11105051]
41. Kuchibhotla KV, et al. Abeta plaques lead to aberrant regulation of calcium homeostasis in vivo resulting in structural and functional disruption of neuronal networks. Neuron. 2008; 59:214–225. [PubMed: 18667150]
42. Hong YK, Kim IJ, Sanes JR. Stereotyped axonal arbors of retinal ganglion cell subsets in the mouse superior colliculus. J Comp Neurol. 2011; 519:1691–1711. [PubMed: 21452242]
43. Meyer-Franke A, Kaplan MR, Pfrieger FW, Barres BA. Characterization of the signaling interactions that promote the survival and growth of developing retinal ganglion cells in culture. Neuron. 1995; 15:805–819. [PubMed: 7576630]
44. Chen Y, et al. NS21: re-defined and modified supplement B27 for neuronal cultures. J Neurosci Methods. 2008; 171:239–247. [PubMed: 18471889]
45. Whitney IE, Keeley PW, Raven MA, Reese BE. Spatial patterning of cholinergic amacrine cells in the mouse retina. J Comp Neurol. 2008; 508:1–12. [PubMed: 18288692]

46. Rodieck RW. The density recovery profile: a method for the analysis of points in the plane applicable to retinal studies. Vis Neurosci. 1991; 6:95–111. [PubMed: 2049333]

47. Montague PR, Friedlander MJ. Morphogenesis and territorial coverage by isolated mammalian retinal ganglion cells. J Neurosci. 1991; 11:1440–1457. [PubMed: 2027055]

48. Smith TG Jr. Lange GD, Marks WB. Fractal methods and results in cellular morphology--dimensions, lacunarity and multifractals. J Neurosci Methods. 1996; 69:123–136. [PubMed: 8946315]

49. Wassle H, Peichl L, Boycott BB. Dendritic territories of cat retinal ganglion cells. Nature. 1981; 292:344–345. [PubMed: 7254331]

50. Kay JN, Voinescu PE, Chu MW, Sanes JR. Neurod6 expression defines new retinal amacrine cell subtypes and regulates their fate. Nature Neurosci. 2011; 14:965–972. [PubMed: 21743471]

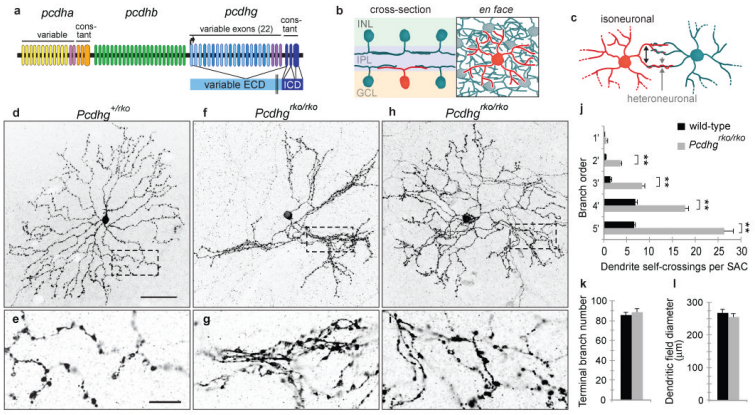

Figure 1. Pcdhgs are required for self-avoidance of SAC dendrites

a. *Pcdh* locus comprises *Pcdha, Pcdhb* and *Pcdhg* subclusters. *Pcdha* and *Pcdhg* isoforms are assembled by splicing of 1 variable exon to 3 constant exons.

b. SACs are present in both inner nuclear and ganglion cell layers (INL, GCL) and extend dendrites that form radially symmetrical arbors confined to thin sublaminae in the inner plexiform layer (IPL).

c. SAC dendrites avoid isoneuronal dendrites but form synapses with dendrites of other SACs.

d-i. Morphology of single SAC, labeled with membrane-Cherry, in the GCL in wild-type and *Pcdhg* mutant retinas. Wild-type SAC dendrites self-avoid. In *Pcdhg* mutants, self-avoidance defects include self-crossing and bundling of dendrites. Crossings are detected at 0.2 μm x-y resolution in single 0.8 μm optical sections (**g,i** magnified inset in **f,h**). Images with 0.2 μm z resolution are shown in Supplementary Fig. 1.

j. SAC dendritic self-crossings in 1st-5th order branches per SAC. Graph underestimates difference between genotypes because the most severely affected mutant SACs could not be scored. ** *P<0.01*

k,l. Number of terminal branches (**i**) and dendritic field diameter (**j**) do not differ between wild-type and mutant SACs. **i-l** show means ±s.e.m; n=8 cells from 5-6 animals per genotype.

Scale bars, 50 μm (**d,f**) or 10 μm (**e,g**).

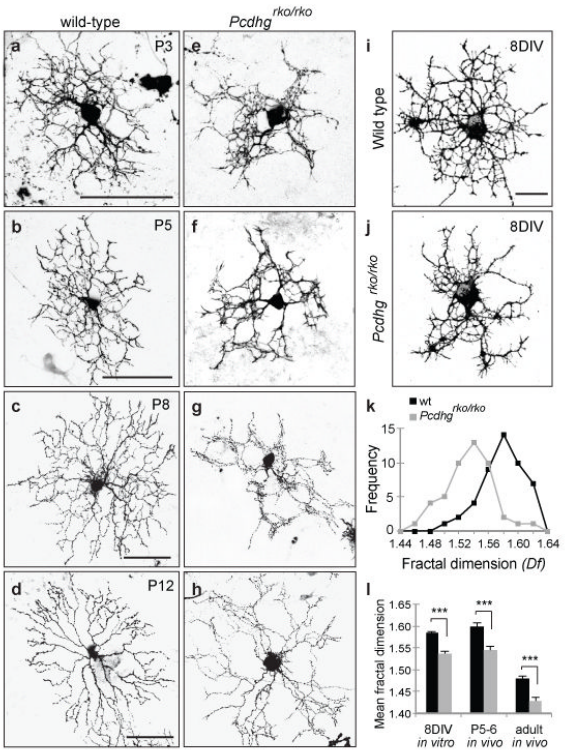

Figure 2. Pcdhgs pattern developing SAC dendrites in a cell-autonomous manner

a-h. SACs in developing wild-type and *Pcdhg* mutant retinas. Wild-type SACs extend fine, exuberant branches (P3, P5) that make transient intradendritic contacts (P5, P8); by P12, excess branches and isoneuronal contacts are eliminated. Dendrites of mutant SACs display excessive self-crossing and bundling by P3; by P12, excess branches are eliminated, but crossing dendrites remain.

i,j. Cultured *Pcdhg* mutant SACs exhibit loss of symmetric growth and uneven distribution of neurites.

k. Histogram of fractal dimensions (*Df,* metric for space-filling) for 47 wild-type (black) and 47 mutant (grey) SACs. Wild-type SAC in **i** has *Df* of 1.61 and mutant SAC in **j** has *Df* of 1.53.

l. Mean *Df* for cultured SACs (n=47 cells), SACs *in vivo* at P5 (n=6) and adult (n=9). *** *P<0.001.* Error bars, s.e.m. Scale bars, 50 μm except 20 μm in **i,j.**

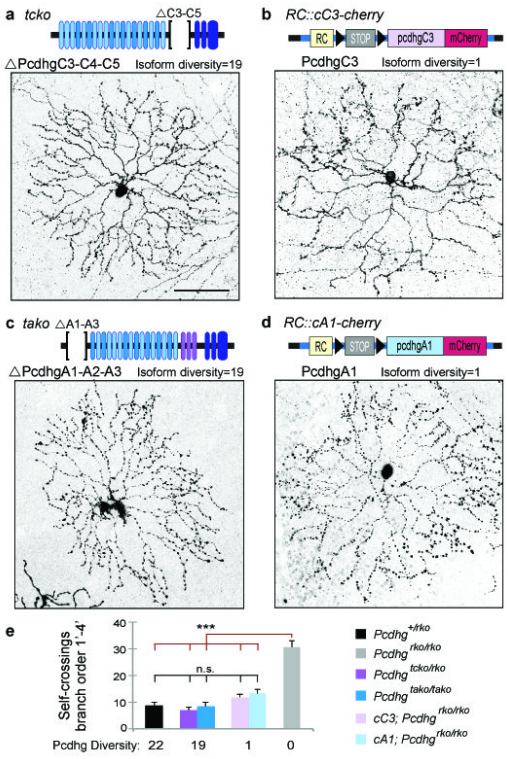

Figure 3. No single Pcdhg isoform is necessary and any isoform is sufficient for dendrite self-avoidance

a. SACs lacking *Pcdhgc3-c5* (*pcdhg*$^{tcko/fcon3}$*;retina-cre*) exhibit self-avoidance.

b. Replacement of all 22 Pcdhgs by the PcdhgC3 isoform rescues SAC dendrite self-avoidance.

c. SACs lacking *Pcdhga1-a3* (*pcdhg*$^{tako/tako}$) exhibit self-avoidance.

d. Replacement of all 22 Pcdhgs by the PcdhgA1 isoform rescues SAC dendrite self-avoidance.

e. Compared to mutants lacking all 22 isoforms, self-crossings in SACs expressing 19 or 1 isoform are restored to control levels. **** P<0.001*; n.s., not significant. Bars are mean ± s.e.m, from 7 SACs from *pcdhg*$^{tcko/fcon3}$*;retina-cre* retinas, 3 SACs from *pcdhg*$^{tako/tako}$, and 9 from remaining genotypes. Scale bars, 50 μm.

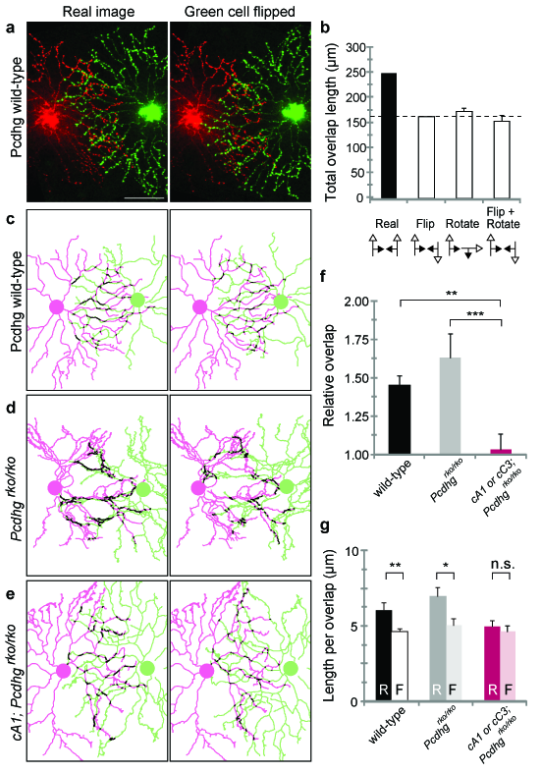

Figure 4. Reducing *Pcdhg* diversity disrupts heteroneuronal SAC interactions

a. Two nearby SACs from a wild-type mouse injected with contrasting fluorescent dyes. Right panel shows image of the green SAC flipped vertically.

b. Overlap between red and green cells in **a**. First two bars are derived from the two panels in **a**. The green cell was rotated in 45° steps or flipped and then rotated; third and fourth bars show mean overlap ± s.e.m. derived from these images (n=7). All inversions and rotations decrease overlap, indicating that overlap in the real image is non-random.

c-e. Tracings of SAC pairs, and versions flipped as in **a**, from wild-type, *Pcdhg*$^{rko/rko}$ and cA1;*Pcdhg*$^{rko/rko}$ mice. Overlap shown in black.

f. Overlap between neighboring cells, expressed as ratio between overlap measured in real and flipped images. Bars show mean ± s.e.m. for 11, 9 and 8 pairs from wild-type, *Pcdhg*$^{rko/rko}$ and single isoform-expressing (cA1;*Pcdhg*$^{rko/rko}$ and cC3;*Pcdhg*$^{rko/rko}$) animals. Expression of a single isoform in neighboring SACs decreases their interaction.

g. Mean length of overlapping segments between SAC pairs. R, real image; F, flipped image. **P=0.05; **P<0.05; ***P<0.01.* Error bars, s.e.m. N as in **f**. Scale bar, 50 μm.

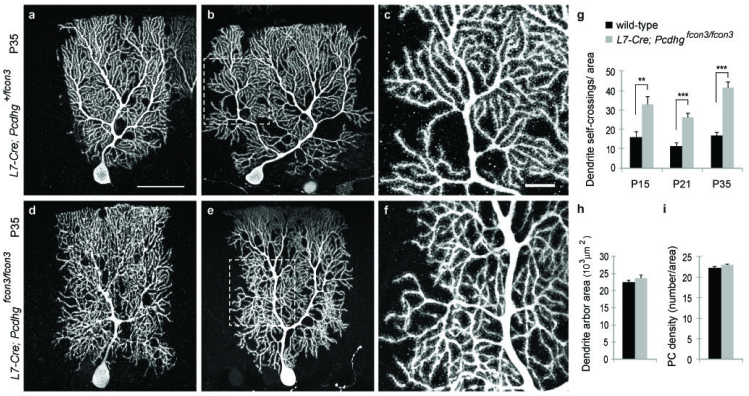

Figure 5. Purkinje cell dendrite self-avoidance requires *Pcdhgs*

a-c. Control Purkinje cells labeled with Cre-dependent AAV-XFP in *L7-cre* transgenic mouse. Self-avoidance is clear in high magnification view in **c** (inset in **b**).

d-f. Purkinje cells lacking Pcdhgs and labeled as in **a-c** have disorganized arbors marked by frequent self-crossing defects. **f** shows area boxed in **e**. **g.** Self-crossings detected in single confocal z-sections of 7225 μm^2 unit area. *** P <0.001; n=8, 15 and 15 cells at P15, P21 and P35 respectively from ≥ 3 mice per genotype. **h,i.** Area of dendritic arbors (n=20 cells) and cell density (>40 regions) do not differ between control and mutant Purkinje cells. Bars show mean ±s.e.m. Scale bars, 50 μm in **a, b, d, e**; 10 μm in **c, f**.